ACCOUNTS
of chemical research

Comprehensive Approach to Intrinsic Charge Carrier Mobility in Conjugated Organic Molecules, Macromolecules, and Supramolecular Architectures

AKINORI SAEKI,[†] YOSHIKO KOIZUMI,[†,‡] TAKUZO AIDA,[‡,§] AND SHU SEKI*[,†]

[†]*Department of Applied Chemistry, Graduate School of Engineering, Osaka University, 2-1 Yamadaoka, Suita, Osaka 565-0871, Japan,* [‡]*Functional Soft Matter Research Group, RIKEN Advanced Science Institute, 2-1 Hirosawa, Wako, Saitama 351-0198, Japan, and* [§]*Department of Chemistry and Biotechnology, School of Engineering, The University of Tokyo, 7-3-1 Hongo, Bunkyo-ku, Tokyo 113-8656, Japan*

RECEIVED ON NOVEMBER 8, 2011

CONSPECTUS

Si-based inorganic electronics have long dominated the semiconductor industry. However, in recent years conjugated polymers have attracted increasing attention because such systems are flexible and offer the potential for low-cost, large-area production via roll-to-roll processing. The state-of-the-art organic conjugated molecular crystals can exhibit charge carrier mobilities (μ) that nearly match or even exceed that of amorphous silicon ($1-10$ cm^2 V^{-1} s^{-1}). The mean free path of the charge carriers estimated from these mobilities corresponds to the typical intersite (intermolecular) hopping distances in conjugated organic materials, which strongly suggests that the conduction model for the electronic band structure only applies to $\mu > 1$ cm^2 V^{-1} s^{-1} for the translational motion of the charge carriers. However, to analyze the transport mechanism in organic electronics, researchers conventionally use a disorder formalism, where μ is usually less than 1 cm^2 V^{-1} s^{-1} and dominated by impurities, disorders, or defects that disturb the long-range translational motion.

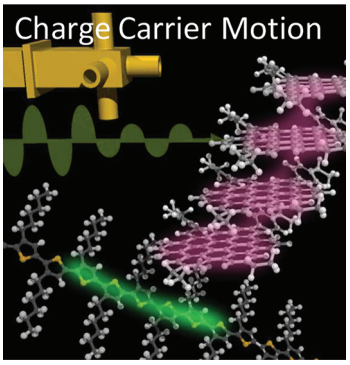

In this Account, we discuss the relationship between the alternating-current and direct-current mobilities of charge carriers, using time-resolved microwave conductivity (TRMC) and other techniques including field-effect transistor, time-of-flight, and space-charge limited current. TRMC measures the nanometer-scale mobility of charge carriers under an oscillating microwave electric field with no contact between the semiconductors and the metals. This separation allows us to evaluate the intrinsic charge carrier mobility with minimal trapping effects.

We review a wide variety of organic electronics in terms of their charge carrier mobilities, and we describe recent studies of macromolecules, molecular crystals, and supramolecular architecture. For example, a rigid poly(phenylene-*co*-ethynylene) included in permethylated cyclodextrin shows a high intramolecular hole mobility of 0.5 cm^2 V^{-1} s^{-1}, based on a combination of flash-photolysis TRMC and transient absorption spectroscopy (TAS) measurements. Single-crystal rubrene showed an ambipolarity with anisotropic charge carrier transport along each crystal axis on the nanometer scale.

Finally, we describe the charge carrier mobility of a self-assembled nanotube consisting of a large π-plane of hexabenzocoronene (HBC) partially appended with an electron acceptor. The local (intratubular) charge carrier mobility reached 3 cm^2 V^{-1} s^{-1} for the nanotubes that possessed well-ordered π-stacking, but it dropped to 0.7 cm^2 V^{-1} s^{-1} in regions that contained greater amounts of the electron acceptor because those molecules reduced the structural integrity of π-stacked HBC arrays. Interestingly, the long-range (intertubular) charge carrier mobility was on the order of 10^{-4} cm^2 V^{-1} s^{-1} and monotonically decreased when the acceptor content was increased. These results suggest the importance of investigating charge carrier mobilities by frequency-dependent charge carrier motion for the development of more efficient organic electronic devices.

Published on the Web 06/07/2012 www.pubs.acs.org/accounts
10.1021/ar200283b

1. Introduction

Many compound and oxide semiconductor materials have been developed over the last 60 years since the discovery of solid state semiconductor devices; however, Si remains the central material and dominates the semiconductor industries.[1] Conjugated organic materials are the most recent candidates to challenge the realm of Si to date, bearing attractive properties such as ease of fabrication, mechanical flexibility, and low cost, which are not common to conventional inorganic semiconductor materials.[2−5] In view of the intrinsic ability of semiconductor devices to modulate or switch electrical currents in these materials, the most important materials parameter is the charge carrier mobility. The key to the successful future of organic semiconductors is to realize a mobility equivalent to that of Si-based materials. Organic conjugated molecular crystals have been reported to often exhibit higher values of mobility (>10 $cm^2\ V^{-1}\ s^{-1}$)[6] than amorphous silicon (1−10 $cm^2\ V^{-1}\ s^{-1}$),[7,8] which is quite reasonable when considering the far higher mobility values reported for carbon-based graphenes,[9] fullerenes,[10] and carbon nanotubes.[11]

Conjugated macromolecules are also powerful candidates as organic semiconductor materials providing conductive pathways along their backbones. Highly sophisticated statistical theories on the supramolecular structure of macromolecules in their solid or solution states have already been developed in the last century, making available the precise prediction of not only the microscopic backbone conformation parameters, such as persistence length, but also macroscopic phase diagrams or rheological parameters. Flexible backbone architectures are advantageous for the fabrication of materials into devices; however, this can disturb the effective charge carrier transport pathways along the backbones. Thus, conjugated semiconductor macromolecules have been developed based on a guiding principle of balancing the flexible chain conformation and the secure effective pathways, which is in striking contrast to the principle for small conjugated molecular materials or supramolecular architectures of providing perfectly ordered structures for charge carrier transport. This implies that the conventional approaches to charge carrier mobility have buried the intrinsic nature of the conjugated backbones, and in this Account, we focus on the recent progress of novel methodologies that reveal the intrinsic charge carrier transport properties in organic molecular/supramolecular/macromolecular materials.

2. Comprehensive Approach to Charge Carrier Mobility

In electrically conductive materials, the charge carrier mobility (μ) is directly related to the electrical conductivity (σ) as follows:

$$\sigma = en\mu \tag{1}$$

where e and n are the elementary charge and density of the charge carriers. In thermal equilibrium, the mean velocity of charge carriers (v_t) is given as a function of temperature (T) with the Boltzmann constant (k),

$$\frac{1}{2}mv_t^2 = \frac{3}{2}kT \tag{2}$$

Thus, the mean free path of the charge carriers (l) in the medium is defined as a function of v_t:

$$l = 2\tau v_t \tag{3}$$

where τ is the relaxation time reflecting the collision interval in the translational motion of charge carriers in the valence or conduction bands. Based on eqs 2 and 3, l is related to τ as follows:

$$l = 2\tau\left(\frac{3kT}{m}\right)^{1/2} \tag{4}$$

In the case of direct-current conduction of charge carriers under an externally applied electric field (E), the current density (J) is denoted by

$$J = nev_t \tag{5}$$

based on the classical Ohm's law

$$J = \sigma E \tag{6}$$

and thus combining eqs 1, 5, and 6 leads to the following formulations of v_τ and μ as

$$v_t = \frac{e\tau}{m}E \tag{7}$$

$$\mu = \frac{e\tau}{m} \tag{8}$$

Mobility is directly related to the mean free path as

$$\mu \approx \frac{el}{(2\pi mkT)^{1/2}} \tag{9}$$

Based on eq 9, the mobility of $\mu \approx 1\ cm^2\ V^{-1}\ s^{-1}$ is estimated under the assumptions of $T = 300$ K and $l = 1$ nm, which is the typical intersite (intermolecular) hopping distance in conjugated organic materials. This strongly suggests that the conduction model for the electronic band structure is applicable only for μ over 1 $cm^2\ V^{-1}\ s^{-1}$ for the translational motion of the charge carriers. Hall effect and field effect transistor (FET) measurements are the appropriate methodologies to estimate the charge carrier mobility in this range.

For the case of $\mu < 1$ cm^2 V^{-1} s^{-1}, the following sophisticated form of expression has been developed and provides a good interpretation of the hopping transport of charge carriers in condensed organic matter:[12]

$$\mu(T,E) = \mu_0 \exp\left(-\frac{\varepsilon_0 - \beta\sqrt{E}}{kT_{\text{eff}}} \right)$$

$$1/T_{\text{eff}} = 1/T - 1/T_0 \qquad (10)$$

where ε_0, β, and T_0 are the zero-field activation energy for the hopping process, the Poole−Frenkel constant, and the equivalent temperature where the Arrhenius dependence is convergent for all electric field strengths, respectively. Time-of-flight (TOF) measurements for charge carrier transport in bulk organic conjugated materials are among the most reliable methods to estimate mobility based on the long-range translational motion of carriers, and the formulation given in eq 10 has often been the first choice to analyze the transport mechanism. However, organic bulk materials contain considerable amounts of impurities, disorders, or defects, which disturb the long-range translational motion. This leads to serious deformation of the transient photocurrent traces observed in the media, and the mobility estimated based on the eq 10 becomes misleading. Taking into account the effects ascribed to disordered structures, a disorder formalism has been developed and successfully applied to the analysis of photocurrent traces. The distribution of the energy levels of hopping sites were parametrized into σ_t, and the spatial distribution of the sites as $\mathbf{\Sigma}_t$, and the overall dependence of μ on E and T was given by[13]

$$\mu(T,E) = \mu_0 \exp\left[-\left(\frac{2\sigma_t}{3kT}\right)^2 \right] \times \exp\left[C\left\{ \left(\frac{\sigma_t}{kT}\right)^2 - \mathbf{\Sigma}_t{}^2 \right\}\sqrt{E} \right] \qquad (11)$$

This formulation provides a powerful analysis for charge carrier transport mechanisms with quantitative estimates of disordered structures in the media. As seen from eq 11, the actual values of mobility are strongly dependent on E and T, which suggests that the value of charge carrier mobility is not unique for hopping transport in the media.

On the other hand, the complex dielectric constant of media with low electrical conductivity σ is deduced from Maxwell equation,

$$\varepsilon = \varepsilon_m - i\frac{\sigma}{\omega} \qquad (12)$$

This leads to a direct correlation with the complex dielectric constant and the conductivity of the material, and the charge carrier mobility can be estimated quantitatively without using electrodes by a precise analysis of the differential changes in the complex dielectric constant attributed to the transient charge carriers injected into the material.

3. Noncontact Mode Conductivity Measurement

3.1. General Introduction to Dielectric Loss Spectroscopy. Dielectric loss spectroscopy using a large library of electromagnetic waves have been used for several decades to investigate the interaction of matter.[14,15] In particular, the complex dielectric constant is one indicator of dielectric loss and relaxation processes. Warman and colleagues at Delft University of Technology have proposed an electrical conductivity measurement technique based on the use of microwaves and pulsed radiation,[16,17] which is referred to as pulse-radiolysis time-resolved microwave conductivity (PR-TRMC), because it generates transient charge carriers in the material upon exposure to a pulsed high-energy electron beam. The density of the generated charge carriers can be determined without performing any other independent measurements, due to the homogeneous ionization of the primary component of the media, which allows direct evaluation of the charge carrier mobility from accurate detection of the dielectric loss. In contrast, the authors have focused on a flash-photolysis TRMC (FP-TRMC) technique that utilizes exciton dissociation into charges as a charge carrier injection scheme.[18,19] By combination with transient absorption spectroscopy (TAS), FP-TRMC provides a versatile route toward the elucidation of intrinsic charge carrier mobility in a wide variety of organic and inorganic electronic materials. Figure 1 shows a schematic of the FP-TRMC system using 9 GHz microwaves.

The present FP-TRMC system adopts a resonant cavity as an interaction site between the sample and microwave. In a resonant cavity, the microwaves can be regarded as standing waves and not traveling waves, which leads to a simple form of the electric field function that depends only on spatial coordinates. A benefit of the resonant cavity is that the degree of microwave probe interactions with the sample is progressively increased. For instance, the number exceeds

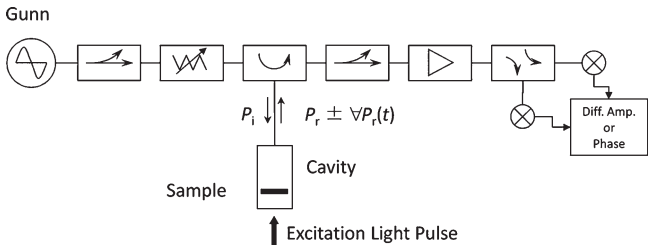

FIGURE 1. Block diagram of the FP-TRMC system using 9 GHz (X-band) microwaves.

ca. 2500 in the present FP-TRMC system, which corresponds to the Q value ($=f_0/\Delta f_0$, f_0 is a resonant frequency, and Δf_0 is the full-width at half-maximum of a Q curve) of the cavity. This represents a 3 orders of magnitude increase in sensitivity in comparison with a typical dielectric loss measurement as a trade-off for the loss of time resolution.

Hereafter, we introduce recent examples of FP-TRMC measurements of conjugated materials. Many conjugated polymer backbones have been explored with the aim of producing novel organic semiconductors. FP-TRMC probes vibrational charge carrier motion in a conjugated polymer within a limited space. The spatial deviation of charge carrier motion (dx) is given by

$$dx \approx \frac{2\pi\mu E}{\omega} \tag{13}$$

If we suppose that $\mu = 1\ \mathrm{cm^2\ V^{-1}\ s^{-1}}$ and $E = 10\ \mathrm{V\ cm^{-1}}$ (the minimum strength of the electric field in TRMC), then eq 13 yields $dx = 0.01$ nm for one charge carrier motion. The motion can be regarded as uniform in an isotropic medium, because the photogenerated charge carrier density is as small as the picomole level (based on assumptions that the charge carrier generation efficiency ϕ is 10^{-5} and the incident laser intensity I_0 is $10^{15}\ \mathrm{cm^{-2}}$). The ϕ is defined as the quantum yield of charge carrier generation per one incident photon absorption at the pulse end of FP-TRMC kinetics. In the next subsection, the transient photoconductivity, $\Delta\sigma$ in $\mathrm{S\ m^{-1}}$ units, is converted to $\phi\Sigma\mu$ in $\mathrm{cm^2\ V^{-1}\ s^{-1}}$ units, where $\Sigma\mu$ represents the sum of hole and electron mobilities ($\mu_h + \mu_e$). Thus, independent estimation of ϕ is necessary for the determination of $\Sigma\mu$.

By taking account of the above-mentioned Q value, the local oscillational motion of charge carriers is estimated to be ca. 1 nm by multiplying the number of dispersions accompanied by interactions between the charge carriers and microwaves. This value is equivalent to a length of a few to tens of monomer units in a conjugated polymer and to the persistent length, L_p, of a polymer backbone (e.g., persistent length of θ condition of polystyrene in cychlohexane). The L_p is responsible for the delocalization of π-orbital on the conjugated polymer chain, having a significant impact on the band gap and charge migration. Consequently, FP-TRMC allows for revealing the intrinsic nature of intramolecular charge carrier transport, due to the probing spatial scale relevant to L_p.

Table 1 lists the charge carrier mobilities and anisotropic mobilities of categorized organic semiconductors measured using PR-TRMC or FP-TRMC, in addition to reported DC charge carrier mobilities determined by techniques such as FET, TOF, and space-charge-limited current (SCLC). In the next subsection, we introduce three example materials: polymer, crystal, and supramolecular architecture.

3.2. Poly(phenylene-*co*-ethynylene) Included in Permethylated Cyclodextrin. Simultaneous estimation of the charge carrier density (n in eq 1) is necessary with FP-TRMC measurements for assessment of the charge carrier mobility. Here we used TAS for this purpose, which is also an electrodeless measurement method that provides information regarding the time evolution of the charge carrier density. Figure 2 shows FP-TRMC and TAS transients for a rigid poly(phenylene-*co*-ethynylene) (PE).[28] Generally, PE without flexible substituents is not suitable for film preparation and TAS, due to its low solubility; however, inclusion in permethylated cyclodextrin affords high solubility and transparency, as well as retainability of long persistent length and elimination of intermolecular interactions. It is noteworthy that TRMC and TAS transients are identical as shown in Figure 2a. The intensity of TAS spectrum centered at 600 nm (Figure 2b) was enhanced by mixing an electron acceptor, perylenedicarboximide (PDI) derivative, into the PE film accompanied with the appearance of PDI radical anion at ca. 720 nm. These results corroborate that both TRMC and TAS transients are attributed to holes (radical cation) in PE, in accordance with the perfect consistency of the decays. Accordingly, the ϕ can be experimentally estimated from the TAS analysis on the basis of charge carrier equilibrium in the system. The resultant hole mobility was $\mu_h = 0.5\ \mathrm{cm^2\ V^{-1}\ s^{-1}}$, which yields charge carrier displacement length of 5−10 repeating cyclodextrin units using eq 13 and following discussion.[28]

3.3. Single-Crystal Rubrene. Organic single crystals composed of π-conjugated molecules exhibit excellent optical and electrical properties, due to their uniform and periodic configuration. Figure 3a,b shows good coincidence between the FP-TRMC and TAS transients for a rubrene single crystal, which suggests that both of the signals originate from the charge carriers.[42] It is noteworthy that the decay rates of both transients were accelerated with an increase of the excitation laser power. This is a signature of bulk charge recombination. Another advantage of not using electrodes is the speed of the

TABLE 1. Charge Carrier Mobilities Measured by TRMC and DC Techniques

category	materials, conditions	$\Sigma\mu$[a] ($cm^2\ V^{-1}\ s^{-1}$)	estimation method of charge carrier density (or ϕ_{max})[b]	$\phi\Sigma\mu_{max}$[c] ($cm^2\ V^{-1}\ s^{-1}$, λ_{ex})	DC mobility[d] ($cm^2\ V^{-1}\ s^{-1}$)	TRMC anisotropy	ref[e]
polythiophene	rr-P3HT	0.12	TAS_{PDI}	4.0×10^{-4}	(FET_h) 0.1, 2.9×10^{-3}		20−22
	rra-P3HT	0.006	TAS_{PDI}	5.0×10^{-5}	(FET_h)		20,
	P3HT in benzene	0.014−0.02 (1D)	PR		4.3×10^{-6}		22, 23
	rr-P3HT/PCBM	>0.22	I_0 dependence	4.5×10^{-3}	($SCLC_h$) 6×10^{-5}		24, 25
	self-threading PT	0.9 (1D)	DC	3.9×10^{-4}	($SCLC_e$) 7×10^{-5}		26
poly(phenylene vinylene)	MEH-PPV in benzene	0.43 (1D)	PR		(TOF_h) 2.1×10^{-7}		23, 27
	film for DC				(FET) 1×10^{-4}		
poly(phenylene ethynylene) (PPE)	rotaxane structure for TRMC, normal alkoxy-PPE for DC	0.5 (1D)	DC, TAS	5×10^{-3}	(TOF_h) 2.2×10^{-3} (TOF_e) 1.8×10^{-3}		28, 29
polyfluorene	PDEHF in benzene (Bz) or *trans*-decalin(TD) film for DC	0.74 (1D, Bz), 0.44 (1D, e, TD), 0.52 (1D, h, TD)	PR	$(0.75 \pm 0.25) \times 10^{-4}$	(TOF_h) 8×10^{-3} (TAS) 3.5×10^{-3}	7 (aligned film)	23, 30−33
fluorene−thiophene copolymer	F8T2	0.83 (1D)	DC	9.5×10^{-5}	(FET_h) 0.01−0.02		34, 35
ladder polymer	poly(*p*-phenylenes)	0.025−0.24, 600 (1D)[f]	PR		(TOF_h) 3.7×10^{-3}		36, 37
polysilane	poly(hexylphenyl)-silane in benzene	0.30 (1D)	PR		(TOF_h) 2.8×10^{-3}		23, 38, 39
acene film, crystal	pentacene film	>0.7	TAS	1.9×10^{-3} (193 nm)	(FET_h) 3.6		40, 41
	rubrene single crystal (SC)	0.052	TAS	3.2×10^{-3}	(FET_h) 43	2.3	42, 43
	aryl−perfluoroaryl substituted tetracene SC			7.0×10^{-4}	(FET_h) 4.2×10^{-2}	2.5	44
molecular crystals	sumanene	0.75 (1D)	TAS	4.5×10^{-2}	(FET_h) 1.1×10^{-5}	9.2	45
	dehydrobenzo[12]annulene	0.15 (1D)	DC	6.5×10^{-3}		12	46
	thiophene−phenylene cooligomer	>0.12	TAS	3.0×10^{-3}	(FET_h) 1.7×10^{-3}		47, 48
	trifluoroacetyl-thiophene/phenylene cooligomer	2.4(1D)	DC	2.0×10^{-2}	(FET_e) 0.2		49
	perylenediimide (PDI)	0.1−0.2	PR		(FET_e) 0.11−0.69		50, 51

TABLE 1. Continued

category	materials, conditions	$\Sigma\mu$[a] ($cm^2\ V^{-1}\ s^{-1}$)	estimation method of charge carrier density (or ϕ_{max})[b]	$\phi\Sigma\mu_{max}$[c] ($cm^2\ V^{-1}\ s^{-1}$, λ_{ex})	DC mobility[d] ($cm^2\ V^{-1}\ s^{-1}$)	TRMC anisotropy	ref[e]
$La@C_{82}$	10 ± 5 (1D)	DC	5.7×10^{-3} (532 nm)	(TOF_e) $(8.0 \pm 2.4) \times 10^{-2}$	7.1	52	
HBC	HBC-TNF coassembled NT	0.7–3.0 (1D)	TAS	2.9×10^{-2}	(FET_h) $1.3–2.3 \times 10^{-4}$	10	53, 54
	HBC-C_{60} coassembled NT	2.0 (1D)	TAS	5.9×10^{-2}	(FET_h) $<1.1 \times 10^{-4}$		55
	HBC Col_h (hydrophobic side-chains)	0.26–1.00 (1D)	PR		(FET_e) $<1.1 \times 10^{-5}$ (FET_h) 1.0×10^{-3}		56, 57
liquid crystal	fused porphyrin	0.27 (1D)	TAS	2.4×10^{-4}	(TOF_h) 4.3×10^{-3}		58
	triphenylene	0.3–0.4 (1D)	PR		(TOF_e) 1.3×10^{-3} (TOF_h) ~0.1		59
D/A dyad	thiophene/PDI			6.6×10^{-4}	(FET_h) 1.0×10^{-4}		60, 61
	thiophene/PDI dendrimer	0.013	TAS_{PDI}	4.6×10^{-4}	(FET_e) 9.8×10^{-7}		62
	porphyrin/C_{60} block-copolymer	0.26	DC	6.4×10^{-4}	(TOF_h) 0.037 (TOF_e) 3×10^{-3}		63

[a] 1D represents one-dimensional mobility, which is calculated by multiplying the obtained $\Sigma\mu$ by a factor of 3 (in the case of the HBC nanotube, by a factor of 2). Others are isotropic values (three-dimensional mobility). [b] TAS = transient absorption spectroscopy. TAS_{PDI} represents the estimation of ϕ_{max} based on the incorporated perylenebisimide (PDI) radical anion. PR = pulse radiolysis. DC = direct current technique using a contact-mode device. I_0-dependence = saturated $\phi\Sigma\mu_{max}$ at low laser power (I_0), the value of which gives the minimum mobility. [c] λ_{ex} is the wavelength of the excitation laser (355 nm unless otherwise noted). [d] Direct current (DC) mode mobility. FET = field-effect transistor, TOF = time-of-flight, SCLC = space-charge-limited current, TAS = transient absorption spectroscopy (not DC method). The subscript of the abbreviation represents the polarity of the charge carrier (h = hole, e = electron). [e] The bold reference numbers report TRMC and others report DC mobility. [f] The value 0.025–0.24 $cm^2\ V^{-1}\ s^{-1}$ was experimentally observed for 13–54 repeating units; 600 $cm^2\ V^{-1}\ s^{-1}$ was deduced from fitting to the theoretical equation of frequency-dependent mobility.

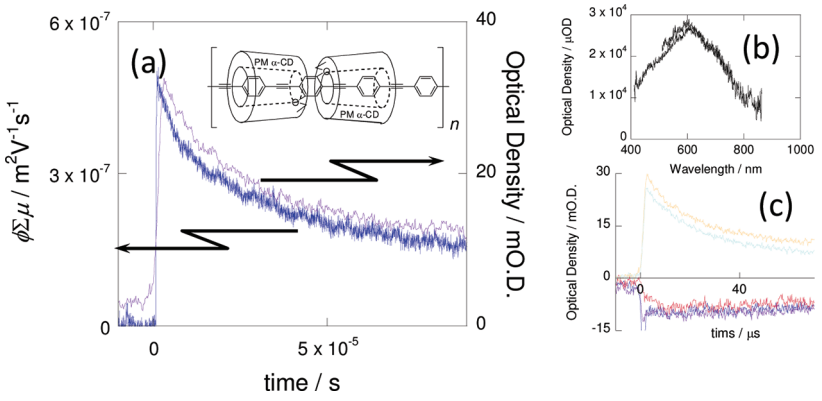

FIGURE 2. (a) FP-TRMC (blue) and TAS (purple, at 600 nm) transients of PE insulated by permethylated cyclodextrin. (b) TAS spectrum of PE film at 2 μs delay after the pulse. (c) TAS kinetic traces of PE film in the presence of 2.5 mol % PDI. The orange, light-blue, blue, purple, and red lines represent the decays at 600, 700, 430, 420, and 410 nm, respectively. Reproduced with permission from ref 28. Copyright 2009 American Chemical Society.

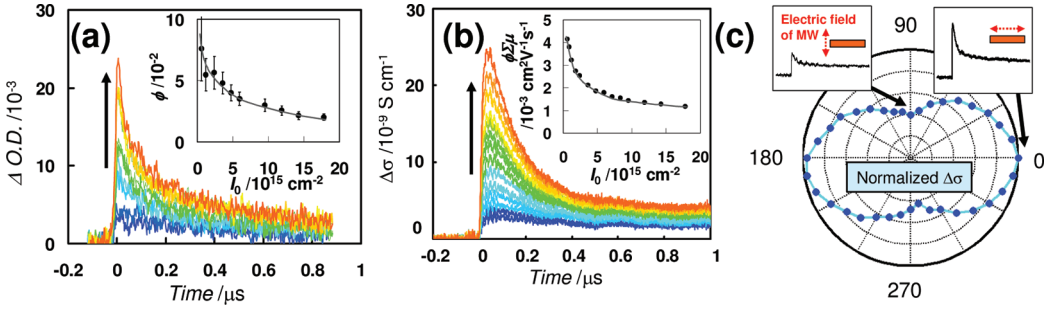

FIGURE 3. Charge carrier dynamics in a rubrene single crystal. (a) TAS profile at 835 nm. I_0 represents the excitation laser power. (b) FP-TRMC transient. (c) Anisotropic photoconductivity. Reproduced with permission from ref 42. Copyright 2008 Wiley-VCH Verlag GmbH & Co. KGaA.

anisotropy measurement with high angle-resolution, because the direction of the electric field of microwaves is fixed along one direction in a resonant cavity. Figure 3c presents the 360° anisotropic conductivity measurement of a rubrene single crystal with an anisotropic ratio of 2.3.

However, the charge carrier mobility estimated from TRMC ($\phi\ \Sigma\mu$), TAS (ϕ), and pulse radiolysis (assignment of absorption spectra of radical cation/anion and their extinction coefficients) was as small as 0.052 $cm^2\ V^{-1}\ s^{-1}$, while the highest FET mobility was reported to be 43 $cm^2\ V^{-1}\ s^{-1}$.[43] This contradiction is discussed with respect to the difference in charge carrier density[64] and frequency-dependent charge carrier motion.[36] Regarding the former, a high density of carriers injected from the electrodes of a FET device can fill the trap sites and lead to trap-free charge carrier motion, while the carrier density in FP-TRMC generated by pulsed laser is more than 3 orders of magnitude smaller than that for a FET. The latter point corresponds to the situation where charge carrier motion with extremely high mobility cannot induce dielectric loss as understood by the combination of real and imaginary parts of conductivity[65] or mobility.[66] Detailed investigation of the frequency-dependent mobility is required to address this problem.

3.4. Photoconductivity of Self-Organized D/A Nanotubes. π-Conjugated dyads of electron donors (D) and acceptors (A) have been the focus of significant attention to provide the ideal structure for an organic photovoltaic cell (OPV). The simple mixing of a D polymer and A molecule, commonly referred to as a bulk heterojunction (BHJ), forms an interpenetrating network with a large interfacial cross section of D/A and efficient charge carrier transport pathways.[67] The bottom-up approach including a self-assembled nanostructure and columnar liquid crystal may open up opportunities to create a discrete p/n junction, thereby widening the scope for potential applications of OPV.

Gemini-shaped hexa-*peri*-hexabenzocoronene (HBC) amphiphiles appended with trinitrofluorenone (TNF) have demonstrated self-assembly to form a coaxial nanotubular structure consisting of π-stacks of a HBC core laminated by TNF outer/inner layers (Figure 4a).[68] Co-assembled engineering of HBC–TNF and HBC led to excellent optoelectronic performance depending on the HBC–TNF content (Figure 4b).[69] Simultaneous measurements of FP-TRMC and TAS revealed that the one-dimensional charge carrier mobility along the long axis of the nanotubes was 3 $cm^2\ V^{-1}\ s^{-1}$.[53]

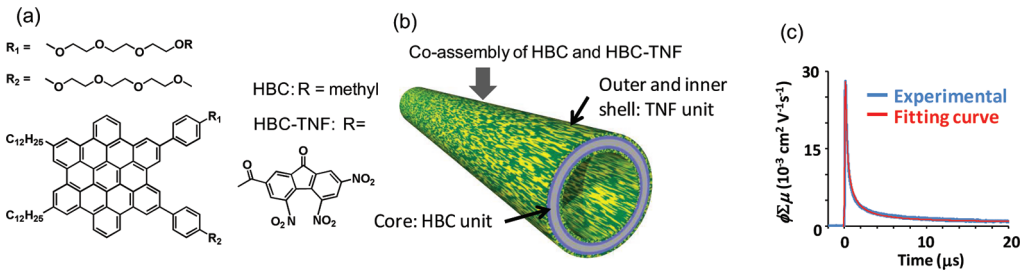

FIGURE 4. (a) Chemical structure of amphiphilic HBC and TNF. (b) Structure of a coassembled nanotube consisting of HBC and HBC–TNF. (c) FP-TRMC transient (blue) and analytical fitting (red). Reproduced with permission from ref 53. Copyright 2011 American Chemical Society.

However, the mobility was considerably dependent on the HBC–TNF content and the size of the acceptor. Co-assembled nanotubes of HBC–C_{60} = 10% had a mobility of 2 $cm^2\ V^{-1}\ s^{-1}$,[55] while the mobility for HBC–TNF = 100% was much smaller (0.7 $cm^2\ V^{-1}\ s^{-1}$). This is rationalized by scanning electron microscopy (SEM) and transmission electron microscopy (TEM) observations, where nanotubes with a high content of HBC–TNF or the presence of HBC–C_{60} exhibit poor structural integrity of the π-stacked HBC arrays. Instead, a high content of HBC–C_{60} can facilitate electron transport on the nanotube surface, as is evident from FET studies. These results clearly suggest that FP-TRMC probes the intratubular charge carrier transport, which reflects the electronic quality of the π-stacks. Furthermore, the FP-TRMC decays of the coassembled nanotubes can be analyzed using a modified analytical solution of first- and second-order differential equations (Figure 4c). The charge carrier mobility derived from the second-order rate constant of the bulk charge recombination was 1.5×10^{-4} $cm^2\ V^{-1}\ s^{-1}$, which is consistent with the FET mobility and suggests a large intertubular hopping barrier.[54] It is of interest that the FET mobility decreases with increasing length of the hydrophobic alkyl chains at the HBC core. In sharp contrast, the TRMC mobility increases with chain length. This is a case of molecular design where maximization of the intra- and intermolecular charge transport is in a trade-off relationship. Insight into the charge carrier motion on local and long-range scales could provide information that would allow the mitigation of barriers for the construction of ideal photoresponsive materials.

4. Concluding Remarks

The importance of providing a flat band for charge carriers can be understood from one of the definitions of charge carrier mobility expressed by

$$\mu = \frac{e\tau}{m_{\mathrm{eff}}} \tag{14}$$

where m_{eff} is the effective mass of the charge carrier. The flat band structure reduces m_{eff} and thus increases μ.

In this Account, we showed that TRMC is very useful for direct estimation of the "weight" of charge carriers in an organic conjugated polymer. The next imperative challenge is to identify polymeric backbone structures that can realize efficient charge carrier transport. A comprehensive approach toward charge carrier mobility would open up opportunities to unveil the intrinsic nature of the charge transport properties in organic electronics, thereby widening the scope for their potential applications.

This work was supported by JSPS Funding Program for Next-Generation World-Leading Researches (NEXT Program), PRESTO-JST, and KAKENHI from the MEXT Japan.

BIOGRAPHICAL INFORMATION

Akinori Saeki received a Ph.D. in Applied Chemistry from Osaka University in 2007 and was an Assistant Professor at the Institute of Scientific and Industrial Research, Osaka University, in 2003–2009. Since 2010, he has been Assistant Professor (tenure track) at the Graduate School of Engineering, Osaka University. His research interest is the dynamics of short-lived reactive species in organic semiconductors.

Yoshiko Koizumi received a Ph.D. in Applied Chemistry from Osaka University in 2008. She had worked for Mitsubishi Chemical Corporation from 2008 to 2011. Since 2011, she has been a postdoctoral fellow of the Functional Soft Matter Research Group at the Advanced Science Institute of RIKEN. Her research interests include the synthesis and characterization of new functional materials for organic semiconductors.

Takuzo Aida received his Ph.D in Polymer Chemistry from the University of Tokyo in 1984. He then began his academic career at the same university and developed precision polymer synthesis with metalloporphyrin complexes. In 1996, he was promoted to Full Professor of the Department of Chemistry and Biotechnology, School of Engineering, the University of Tokyo. His research interests include (1) electronic and optoelectronic soft materials, (2) bioinspired dendritic macromolecules, (3) molecular and biomolecular machines, and (4) biorelated molecular recognition and catalysis.

Shu Seki graduated from the University of Tokyo in 1991 and received a Dr. of Engineering from Osaka University in 2001.

He joined the Chemistry Division of Argonne National Laboratory in 1995 and Delft University of Technology in 2000 as a visiting scientist. Since 2009, he was appointed as a Professor of Chemistry at the Graduate School of Engineering, Osaka University. His research interest is functional polymer science.

FOOTNOTES

*To whom correspondence should be addressed. E-mail: seki@chem.eng.osaka-u.ac.jp.
The authors declare no competing financial interest.

REFERENCES

1 International Technology Roadmap for Semiconductors (ITRS), 2010 ed.; http://www.itrs.net/.

2 Chiang, C. K.; Fincher, C. R., Jr.; Park, Y. W.; Heeger, A. J.; Shirakawa, H.; Louis, E. J.; Gau, S. C.; MacDiarmid, A. G. Electrical Conductivity in Doped Polyacetylene. *Phys. Rev. Lett.* **1977**, *39*, 1098–1101.

3 Brédas, J.-L.; Norton, J. E.; Cornil, J.; Corpceanu, V. Molecular Understanding of Organic Solar Cells: The Challenges. *Acc. Chem. Res.* **2009**, *42*, 1691–1699.

4 Liang, Y.; Yu, L. A New Class of Semiconducting Polymers for Bulk Heterojunction Solar Cells with Exceptionally High Performance. *Acc. Chem. Res.* **2010**, *43*, 1227–1236.

5 Takimiya, K.; Shinamura, S.; Osaka, I.; Miyazaki, E. Thienoacene-Based Organic Semiconductors. *Adv. Mater.* **2011**, *23*, 4347–4370.

6 Podzorov, V.; Menard, E.; Borissov, A.; Kiryukhin, V.; Rogers, J. A.; Gershenson, M. E. Intrinsic Charge Transport on the Surface of Organic Semiconductors. *Phys. Rev. Lett.* **2004**, *93*, No. 086602.

7 Le Comber, P. G.; Spear, W. E. Electronic Transport in Amorphous Silicon Films. *Phys. Rev. Lett.* **1970**, *25*, 509–511.

8 Jüska, G.; Arlauskas, K; Viliunas, M. Extraction Current Transients: New Method of Study of Charge Transport in Microcrystalline Silicon. *Phys. Rev. Lett.* **2000**, *84*, 4946–4949.

9 Novoselov, K. S.; Geim, A. K.; Morozov, S. V.; Jiang, D.; Zhang, Y.; Dubonos, S. V.; Grigorieva, I. V.; Firsov, A. A. Electric Field Effect in Atomically Thin Carbon Films. *Science* **2004**, *306*, 666–669.

10 Singha, Th. B.; Sariciftci, N. S.; Yang, H.; Yang, L.; Plochberger, B.; Sitter, H. Correlation of Crystalline and Structural Properties of C_{60} Thin Films Grown at Various Temperature with Charge Carrier Mobility. *Appl. Phys. Lett.* **2007**, *90*, No. 213512.

11 Dulrkop, T.; Getty, S. A.; Cobas, E.; Fuhrer, M. S. Extraordinary Mobility in Semiconducting Carbon Nanotubes. *Nano Lett.* **2004**, *4*, 35–39.

12 Gill, W. D. Drift Mobilities in Amorphous Charge Transfer Complexes of Trinitrofluorenone and Polynvinylcarbazole. *J. Appl. Phys.* **1972**, *43*, 5033–5040.

13 Bässler, H. Charge Transport in Disordered Organic Photoconductors a Monte Carlo Simulation Study. *Phys. Status Solidi B* **1993**, *175*, 15–56.

14 Biondi, M. A.; Brown, S. C. Measurements of Ambipolar Diffusion in Helium. *Phys. Rev.* **1949**, *75*, 1700–1705.

15 Warman, J. M.; Fessenden, R. W. Three Body Electron by Nitrous Oxide. *J. Chem. Phys.* **1968**, *49*, 4718–4719.

16 Warman, J. M.; Gelinck, G. H.; de Haas, M. P. The Mobility and Relaxation Kinetics of Charge Carriers in Molecular Materials Studied by Means of Pulse-Radiolysis Time-Resolved Microwave Conductivity: Dialkoxy-Substituted Phenylene-Vinylene Polymers. *J. Phys.: Condens. Matter* **2002**, *14*, 9935–9954.

17 Schouten, P. G.; Warman, J. M.; de Haas, M. P. Effect of Accumulated Radiation Dose on Pulse Radiolysis Conductivity Transients in a Mesomorphic Octa-&alkoxy-Substituted Phthalocyanine. *J. Phys. Chem.* **1993**, *97*, 9863–9870.

18 Saeki, A.; Seki, S; Sunagawa, T; Ushida, K; Tagawa, S. Charge-Carrier Dynamics in Polythiophene Films Studied by In-Situ Measurement of Flash-Photolysis Time-Resolved Microwave Conductivity (FP-TRMC) and Transient Optical Spectroscopy (TOS). *Philos. Mag.* **2006**, *86*, 1261–1276.

19 Saeki, A.; Seki, S.; Koizumi, Y; Tagawa, S. Dynamics of Photogenerated Charge Carrier and Morphology Dependence in Polythiophene Films Studied by In-situ Time-Resolved Microwave Conductivity and Transient Absorption Spectroscopy. *J. Photochem. Photobiol. A* **2007**, *186*, 158–165.

20 Saeki, A.; Ohsaki, S.; Seki, S.; Tagawa, S. Electrodeless Determination of Charge Carrier Mobility in Poly(3-hexylthiophene) Films Incorporating Perylenediimide as Photoconductivity Sensitizer and Spectroscopic Probe. *J. Phys. Chem. C* **2008**, *112*, 16643–16650.

21 Sirringhaus, H.; Tessler, N.; Friend, R. H. Integrated Optoelectronic Devices Based on Conjugated Polymers. *Science* **1998**, *280*, 1741–1744.

22 Pandey, S. S.; Takashima, W.; Nagamatsu, S.; Endo, T.; Rikukawa, M.; Kaneto, K. Regioregularity vs Regiorandomneess: Effect on Photocarrier Transport in Poly(3-hexylthiophene). *Jpn. J. Appl. Phys.* **2000**, *39*, L94–L97.

23 Grozema, F. C.; Siebbeles, L. D. A.; Warman, J. M.; Seki, S.; Tagawa, S.; Scherf, U. Hole Conduction along MolecularWires: σ-Bonded Silicon Versus p-Bond-Conjugated Carbon. *Adv. Mater.* **2002**, *14*, 228–231.

24 Saeki, A.; Tsuji, M.; Seki, S. Direct Evaluation of Intrinsic Optoelectronic Performance of Organic Photovoltaic Cells with Minimizing Impurity and Degradation Effects. *Adv. Energy Mater.* **2011**, *1*, 661–669.

25 Park, J. H.; Kim, J. S.; Lee, J. H.; Lee, W. H.; Cho, K. Effect of Annealing Solvent Solubility on the Performance of Poly(3-hexylthiophene)/Methanofullerene Solar Cells. *J. Phys. Chem. C* **2009**, *113*, 17579–17584.

26 Sugiyasu, K.; Honsho, Y.; Harrison, R. M.; Sato, A.; Yasuda, T.; Seki, S.; Takeuchi, M. A Self-Threading Polythiophene: Defect-Free Insulated Molecular Wires Endowed with Long Effective Conjugation Length. *J. Am. Chem. Soc.* **2010**, *132*, 14754–14756.

27 Campbell, I. H.; Smith., D. L.; Neef, C. J.; Ferraris, J. P. Consistent Time-of-Flight Mobility Measurements and Polymer Light-Emitting Diode Current−Voltage Characteristics. *Appl. Phys. Lett.* **1999**, *74*, 2809–2811.

28 Terao, J.; Tanaka, Y.; Tsuda, S.; Kambe, N.; Taniguchi, M.; Kawai, T.; Saeki, A.; Seki, S. Insulated Molecular Wire with Highly Conductive π-Conjugated Polymer Core. *J. Am. Chem. Soc.* **2009**, *131*, 18046–18047.

29 Kokil, A.; Shiyanovskaya, I.; Singer, K. D.; Weder, C. Charge Carrier Transport in Poly(2,5-dialkoxy-p-phenylene ethynylene)s. *Synth. Met.* **2003**, *138*, 513–517.

30 Redecker, M.; Bradley, D. D. C.; Inbasekaran, M.; Woo, E. P. Mobility Enhancement through Homogeneous Nematic Alignment of a Liquid-Crystalline Polyfluorene. *Appl. Phys. Lett.* **1999**, *74*, 1400–1402.

31 Grozema, F. C.; Savenije, T. J.; Vermeulen, M. J. W.; Siebbeles, L. D. A.; Warman, J. M.; Neher, M. D.; nothofer, H. G.; Scherf, U. Electrodeless Measurement of the In-Plane Anisotropy in the Photoconductivity of an Aligned Polyfluorene Film. *Adv. Mater.* **2001**, *13*, 1627–1630.

32 Grozema, F. C.; Warman, J. M. Highly Mobile Electrons and Holes on Polyfluorene Chains Formed by Charge Scavenging in Pulse-Irradiated Trans-Decalin Solutions. *Radiat. Phys. Chem.* **2005**, *74*, 234–238.

33 Asaoka, S.; Takeda, N.; Iyoda, T.; Cook, A. R.; Miller, J. R. Electron and Hole Transport To Trap Groups at the Ends of Conjugated Polyfluorenes. *J. Am. Chem. Soc.* **2008**, *130*, 11912–11920.

34 Saeki, A.; Fukumatsu, T; Seki, S. Intramolecular Charge Carrier Mobility in Fluorene-Thiophene Copolymer Films Studied by Microwave Conductivity. *Macromolecules* **2011**, *44*, 3416–3424.

35 Sirringhaus, H.; Wilson, R. J.; Friend, R. H.; Inbasekaran, M.; Wu, W.; Woo, E. P.; Grell, M.; Bradley, D. D. C. Mobility Enhancement in Conjugated Polymer Field-Effect Transistor through Chain Alignment in a Liquid-Crystalline Phase. *Appl. Phys. Lett.* **2000**, *77*, 406–408.

36 Prins, P.; Grozema, F. C.; Schins, J. M.; Patil, S; Scherf, U.; Siebbeles, L. D. A. High Intrachain Hole Mobility on Molecular Wires of Ladder-Type Poly(p-Phenylenes). *Phys. Rev. Lett.* **2006**, *96*, No. 146601.

37 Hertel, D.; Scherf, U.; Bässler, H. Carrier Mobility in a Ladder-Type Conjugated Polymer. *Adv. Mater.* **1998**, *10*, 1119–1122.

38 Seki, S.; Tagawa, S. Optoelectronic Properties and Nanostructure Formation of σ-Conjugated Polymers. *Polym. J.* **2007**, *39*, 277–293.

39 Kunimi, Y.; Seki, S; Tagawa, S. Investigation on Hole Drift Mobility in Poly(n-hexylphenylsilane). *Solid State Commun.* **2000**, *114*, 469–472.

40 Saeki, A.; Seki, S; Tagawa, S. Electrodeless Measurement of Charge Carrier Mobility in Pentacene by Microwave and Optical Spectroscopy Techniques. *J. Appl. Phys.* **2006**, *100*, No. 023703.

41 Sun, X.; Zhang, L.; Di, C. −a.; Wen, Y.; Guo, Y.; Zhao, Y.; Yu, G.; Liu, Y. Morphology Optimization for the Fabrication of High Mobility Thin-Film Transistors. *Adv. Mater.* **2011**, *23*, 3128–3133.

42 Saeki, A.; Seki, S.; Takenobu, T.; Iwasa, Y.; Tagawa, S. Mobility and Dynamics of Charge Carriers in Rubrene Single Crystals Studied by Flash-Photolysis Microwave Conductivity and Optical Spectroscopy. *Adv. Mater.* **2008**, *20*, 920–923.

43 Yamagishi, M.; Takeya, J.; Tominari, Y.; Nakazawa, Y.; Kuroda, T.; Ikehata, S.; Uno, M.; Nishikawa, T.; Kawase, T. High-Mobility Double-Gate Organic Single-Crystal Transistors with Organic Crystal Gate Insulators. *Appl. Phys. Lett.* **2007**, *90*, No. 182117.

44 Okamoto, T.; Nakahara, K.; Saeki, A; Seki, S; Oh, J. H.; Akkerman, H. B; Bao, Z.; Matsuo, Y. Aryl−Perfluoroaryl Substituted Tetracene: Induction of Face-to-Face $\pi-\pi$ Stacking and Enhancement of Charge Carrier Properties. *Chem. Mater.* **2011**, *23*, 1646–1649.

45 Amaya, T.; Seki, S; Moriuchi, T; Nakamoto, K; Nakata, T; Sakane, H; Saeki, A; Tagawa, S.; Hirao, T. Anisotropic Electron Transport Properties in Sumanene Crystal. *J. Am. Chem. Soc.* **2009**, *131*, 408–409.

46 Hisaki, I.; Sakamoto, Y.; Shigemitsu, H.; Tohnai, N.; Miyata, M.; Seki, S.; Saeki, A.; Tagawa, S. Superstructure-Dependent Optical and Electrical Properties of an Unusual Face-to-Face, π-Stacked, One-Dimensional Assembly of Dehydrobenzo[12]annulene in the Crystalline State. *Chem.—Eur. J.* **2008**, *14*, 4178–4187.

47 Saeki, A.; Seki, S.; Shimizu, Y.; Yamao, T.; Hotta, S. Photogeneration of Charge Carrier Correlated with Amplified Spontaneous Emission in Single Crystals of a Thiophene/Phenylene Co-oligomer. *J. Chem. Phys.* **2010**, *132*, No. 134509.

48 Yamao, T.; Miki, T.; Akagami, H.; Nishimoto, Y.; Ota, S.; Hotta, S. Direct Formation of Thin Single Crystals of Organic Semiconductors onto a Substrate. *Chem. Mater.* **2007**, *19*, 3748–3753.

49 Ie, Y.; Nitani, M; Uemura, T; Tominari, Y; Takeya, J; Honsho, Y; Saeki, A; Seki, S; Aso, Y. Comprehensive Evaluation of Electron Mobility for a Trifluoroacetyl-Terminated Electronegative Conjugated Oligomer. *J. Phys. Chem. C* **2009**, *113*, 17189–17193.

50 Struijk, C. W.; Sieval, A. B.; Dakhorst, J. E. J.; van Dijk, M.; Kimkes, P.; Koehorst, R. B. M.; Donker, H.; Schaafsma, T. J.; Picken, S. J.; van de Craats, A. M.; Warman, J. M.; Zuilhof, H.; Sudhölter, E. J. R. Liquid Crystalline Perylene Diimides: Architecture and Charge Carrier Mobilities. *J. Am. Chem. Soc.* **2000**, *122*, 11057–11066.

51 Wen, Y.; Liu, Y. Recent Progress in n-Channel Organic Thin-Film Transistors. *Adv. Mater.* **2010**, *22*, 1331–1345.

52 Sato, S.; Seki, S.; Honsho, Y.; Wang, L.; Nikawa, H.; Luo, G.; Lu, J.; Haranaka, M.; Tsuchiya, T.; Nagase, S.; Akasaka, T. Semi-metallic Single-Component Crystal of Soluble La@C_{82} Derivative with High Electron Mobility. *J. Am. Chem. Soc.* **2011**, *133*, 2766–2771.

53 Saeki, A.; Yamamoto, Y.; Koizumi, Y.; Fukushima, T; Aida, T.; Seki, S. Photoconductivity of Self-Assembled Hexabenzocoronene Nanotube: Insight into the Charge Carrier Mobilities on Local and Long-Range Scales. *J. Phys. Chem. Lett.* **2011**, *2*, 2549–2554.

54 Yamamoto, Y.; Jin, W.; Fukushima, T; Minari, T; Tsukagoshi, K; Saeki, A.; Seki, S; Tagawa, S; Aida, T. Charge Transport Properties of Hexabenzocoronene Nanotubes by Field Effect: Influence of the Oligoether Side Chains on the Mobility. *Chem. Lett.* **2009**, *38*, 888–889.

55 Yamamoto, Y.; Zhang, G.; Jin, W.; Fukushima, T; Ishii, N; Saeki, A; Seki, S; Tagawa, S; Minari, T.; Tsukagoshi, K.; Aida, T. Ambipolar-Transporting Coaxial Nanotubes with a Tailored Molecular Graphene−Fullerene Heterojunction. *Proc. Natl. Acad. Sci. U.S.A.* **2009**, *106*, 21051–21056.

56 Warman, J. M.; Piris, J.; Pisula, W.; Kastler, M.; Wasserfallen, D.; Müllen, K. Charge Recombination via Intercolumnar Electron Tunneling through the Lipid-like Mantle of Discotic Hexa-alkyl-hexa-peri-hexabenzocoronenes. *J. Am. Chem. Soc.* **2005**, *127*, 14257–14262.

57 van de Craats, A. M.; Stutzmann, N.; Bunk, O.; Nielsen, M. M.; Watson, M.; Müllen, K.; Chanzy, H. D.; Sirringhaus, H.; Friend, R. H. Meso-Epitaxial Solution-Growth of Self-Organizing Discotic Liquid-Crystalline Semiconductors. *Adv. Mater.* **2003**, *15*, 495–499.

58 Sakurai, T.; Tashiro, K; Honsho, Y; Saeki, A.; Seki, S.; Osuka, A.; Muranaka, A.; Uchiyama, M.; Kim, J; Ha, S.; Kato, K.; Takata, M.; Aida, T. Electron- or Hole-Transporting Nature Selected by Side-Chain-Directed π-Stacking Geometry: Liquid Crystalline Fused Metallo-porphyrin Dimers. *J. Am. Chem. Soc.* **2011**, *133*, 6537–6540.

59 van de Craats, A. M.; Warman, J. M.; de Haas, M. P.; Simmerer, J.; Haarer, D.; Schuhmacher, P. The Mobility of Charge Carriers in All Four Phases of the Columnar Discotic Material Hexakis(hexylthio)triphenylene: Combined TOF and PR-TRMC Results. *Adv. Mater.* **1996**, *8*, 823–826.

60 Li, W.-S.; Saeki, A.; Yamamoto, Y.; Fukushima, T; Seki, S.; Ishii, N.; Kato, K.; Takata, M.; Aida, T. Use of Side-Chain Incompatibility for Tailoring Long-Range p/n Heterojunctions: Photoconductive Nanofibers Formed by Self-Assembly of an Amphiphilic Donor-Acceptor Dyad Consisting of Oligothiophene and Perylenediimide. *Chem.—Asian J.* **2010**, *5*, 1566–1572.

61 Balaji, G.; Kale, T. S.; Keerthi, A.; Pelle, A. M. D.; Thayumanavan, S.; Valiyaveettil, S. Low Band Gap Thiophene-Perylene Diimide Systems with Tunable Charge Transport Properties. *Org. Lett.* **2011**, *13*, 18–21.

62 Ie, Y.; Uto, T.; Saeki, A.; Seki, S.; Tagawa, S.; Aso, Y. Photovoltaic Performance and Charge Carrier Mobility of Dendritic Oligothiophene Bearing Perylene bis(dicarboximide) Groups. *Synth. Met.* **2009**, *159*, 797–801.

63 Charvet, R.; Acharya, S; Hill, J. P.; Akada, M.; Liao, M.; Seki, S; Honsho, Y.; Saeki, A; Ariga, K. Block-Copolymer-Nanowires with Nanosized Domain Segregation and High Charge Mobilities as Stacked p/n Heterojunction Arrays for Repeatable Photocurrent Switching. *J. Am. Chem. Soc.* **2009**, *131*, 18030–18031.

64 Goldmann, C.; Krellner, C; Pernstich, K. P; Haas, S.; Gundlach, D. J.; Batlogg, B. Determination of the Interface Trap Density of Rubrene Single-Crystal Field-Effect Transistors and Comparison to the Bulk Trap Density. *J. Appl. Phys.* **2006**, *99*, No. 034507.

65 Papaioannou, J. C.; Patermarakis, G. S.; Karayianni, H. S. Electron Hopping Mechanism in Hematite (α-Fe_2O_3). *J. Phys. Chem. Solids* **2005**, *66*, 839–844.

66 Prins, P.; Grozema, F. C.; Schins, J. M.; Siebbeles, L. D. A. Frequency Dependent Mobility of Charge Carriers along Polymer Chains with Finite Length. *Phys. Status Solidi B* **2006**, *243*, 382–386.

67 Yu, G.; Gao, J.; Hummelen, J. C.; Wudl, F.; Heeger, A. J. Polymer Photovoltaic Cells: Enhanced Efficiencies via a Network of Internal Donor-Acceptor Heterojunctions. *Science* **1995**, *270*, 1789–1791.

68 Yamamoto, Y.; Fukushima, T; Suna, Y; Ishii, N.; Saeki, A.; Seki, S; Tagawa, S; Taniguchi, M.; Kawai, T.; Aida, T. Photoconductive Coaxial Nanotubes of Molecularly Connected Electron Donor and Acceptor Layers. *Science* **2006**, *314*, 1761–1764.

69 Yamamoto, Y.; Fukushima, T.; Saeki, A.; Seki, S; Tagawa, S; Ishii, N; Aida, T. Molecular Engineering of Coaxial Donor-Acceptor Heterojunction by Coassembly of Two Different Hexabenzocoronenes: Graphitic Nanotubes with Enhanced Photoconducting Properties. *J. Am. Chem. Soc.* **2007**, *129*, 9276–9277.